

# On the Spatial Collinear Restricted Four-Body Problem With Non-Spherical Primaries

Md Sanam Suraj · Rajiv Aggarwal · Amit Mittal · Om Prakash Meena · Md Chand Asique

Received: date / Accepted: date

**Abstract** In the present work a systematic study has been presented in the context of the existence of libration points, their linear stability, the regions of motion where the third particle can orbit and the domain of basins of convergence linked to libration points in the spatial configuration of the collinear restricted four-body problem with non-spherical primaries (i.e., the primaries are oblate or prolate spheroid). The parametric evolution of the positions of the libration points as function of the oblateness and prolateness parameters of the primaries and the stability of these points in linear sense are illustrated numerically. Moreover, the numerical investigation shows that the only libration points which lie on either of the axes are linearly stable for several combinations of the oblateness parameter and mass parameter whereas the non-collinear libration points are found linearly unstable, consequently unstable in nonlinear sense also, for

studied value of mass parameter and oblateness parameter. Moreover, the regions of possible motion are also depicted, where the infinitesimal mass is free to orbit, as function of Jacobian constant. In addition, the basins of convergence (BoC) linked to the libration points are illustrated by using the multivariate version of the Newton-Raphson (NR) iterative scheme.

**Keywords** Collinear restricted four-body problem · Equilibrium points · Linear stability · Zero-velocity curves · Basins of Convergence

## 1 Introduction

The restricted problem of the four bodies with various perturbations have been fascinated by a large group of astronomers, researchers and scientists over the globe in few decades. The restricted problem of four bodies in planar case is referred as restricted  $(N + 1)$  where  $N = 3$ , body problem. In this problem the fourth body does not influence the motion of the three primaries, and consequently the fourth particle can be assumed as a dynamical system composed of an infinitesimal mass (i.e., the test particle) together with the three main primaries. The central configuration of the three-body problem contains two type of configurations: the Euler configuration (i.e., straight-line configuration) and the Lagrange configuration (i.e., the equilateral triangle configuration) (see [Leandro \(2006\)](#), [Hamilton \(2016\)](#)). The classical restricted three-body problem with various perturbations has been studied by many researchers in the few decades. For example the existence as well as stability of the equilibrium points (e.g., [Simmons et al. \(1985\)](#), [Abouelmagd \(2012\)](#), [Abouelmagd and Abdullah \(2019a\)](#), [Selim et al. \(2019\)](#)), when the primaries are non spherical in shape (e.g., [Sharma and Subba Rao \(1979\)](#), [Arredondo et al. \(2012\)](#)), the analysis of periodic orbits (e.g., [Abouelmagd et al. \(2019b\)](#)), the

Md Sanam Suraj  
Department of Mathematics, Sri Aurobindo College, University of Delhi, New Delhi-110017, Delhi, India  
E-mail: [mdsanamsuraj@gmail.com](mailto:mdsanamsuraj@gmail.com)  
E-mail: [mdsanamsuraj@aurobindo.du.ac.in](mailto:mdsanamsuraj@aurobindo.du.ac.in)

Rajiv Aggarwal  
Department of Mathematics, Deshbandhu College, University of Delhi, New Delhi-110019, Delhi, India  
E-mail: [rajiv\\_agg1973@yahoo.com](mailto:rajiv_agg1973@yahoo.com)

Amit Mittal  
Department of Mathematics, ARSD College, University of Delhi, New Delhi-110021, Delhi, India  
E-mail: [to.amitmittal@gmail.com](mailto:to.amitmittal@gmail.com)

Om Prakash Meena  
Department of Mathematics, Deshbandhu College, University of Delhi, New Delhi-110019, Delhi, India

Md Chand Asique  
Deshbandhu College, University of Delhi, New Delhi-110019, Delhi, India  
E-mail: [mdchandasique@gmail.com](mailto:mdchandasique@gmail.com)

basins of convergence and classifications of orbits (e.g., [Zotos \(2015a\)](#), [Zotos \(2015b\)](#)) have been studied in restricted three-body problem.

In the few decades, the Lagrange and Euler configurations of the planar restricted four-body problem (PR4BP) have been discussed by various researchers by modifying the effective potential by adding some extra terms which occur due to various perturbations to unveil the existence of equilibrium points and their stability (e.g., [Michalodimitrakis \(1981\)](#), [Kalvouridis et al. \(2006\)](#), [Medvedev and Perov \(2008\)](#), [Baltagiannis and Papadakis \(2011a\)](#), [Barrabés et al. \(2017\)](#), [Suraj et al. \(2018c\)](#)), the study of the motion of the test particle when its mass is variable (e.g., [Suraj et al. \(2019a\)](#), [Suraj et al. \(2018\)](#)), the computations of periodic orbits (e.g., [Baltagiannis and Papadakis \(2011b\)](#), [Palacios et al. \(2019\)](#)), the study of fractal basins of convergence (e.g., [Zotos \(2017a\)](#), [Suraj et al. \(2018b\)](#)), or the study of orbital dynamics of escape and collisions (e.g., [Zotos \(2016\)](#), [Maranhão and Libre \(1998\)](#)).

In various research papers, the scientists have also studied the existence of libration points and their stability in the same dynamical model by taking the shape of primaries. [Asique et al. \(2015\)](#) have studied the existence of libration points in the photogravitational version of the restricted four-body problem when one of the primary is an oblate/prolate spheroid, whereas [Asique et al. \(2016\)](#) have discussed the same model by taking a triaxial rigid body as primary. [Kumari and Kushvah \(2013\)](#) have included the effect of solar wind drag to discuss the libration points and zero velocity surfaces in the restricted problem of four bodies. In Ref. [Zotos \(2015c\)](#), the author has compared the orbital dynamics in three models which describe the various properties of a star cluster which rotates in a circular orbit around its parent galaxy. Moreover, [Zotos and Jung \(2018\)](#) have discussed the orbit and escape dynamics in barred galaxies and illustrated the basins of escape linked to the escape through the escape channels in the vicinity of the libration points  $L_{2,3}$  which are symmetrical in nature and further established the relation with the corresponding distribution of the escape times of the orbits. In [Zotos et al. \(2018\)](#), the motion of the test particle in a non-spinning binary black hole system is investigated numerically when the masses are equal. Further they have classified the initial conditions into three different categories, i.e., bounded, escaping and displaying close encounters by using the smaller alignment index chaos indicator, the orbits are classified into regular, sticky and chaotic.

In the literature, there is plethora of papers available where the spatial collinear restricted four-body problem (CR4BP) has been discussed. Ref. [Arribas et al. \(2016a\)](#), have discussed the planar motion of the infinitesimal body moving under the system of three main primaries situated in a collinear configuration (Euler 1767) with a symmetry and the peripheral primaries are also source of radiation. In addition, they

have considered the case where the gravitational force is less than the radiation force. In the mentioned setup, they have discussed the analytic study of the position and stability of the libration points for the involve parameters. In continuation of their study, Ref. [Arribas et al. \(2016b\)](#) have discussed the out-of-plane libration points, i.e., the equilibrium points which lie out side the configuration plane of primaries in the same dynamical system. [Barrabés et al. \(2017\)](#) have discussed the relative equilibria and their stability of the infinitesimal mass, moving under the gravitational attraction of three primaries which are in a syzygy, under the repulsive Manev potential. [Zotos \(2017b\)](#) has investigated the BoC linked with the equilibrium points by applying the NR iterative scheme in the collinear restricted four-body problem with angular velocity. He has illustrated the parametric evolution of the positions of equilibrium points and their stability when the values of the mass parameter and the angular velocity are considered in the fixed intervals. [Palacios et al. \(2019\)](#) have illustrated the evolution of families of symmetric periodic orbits as the function of mass parameter and evolution of spiral points, which show the connection between heteroclinic orbits and equilibrium points. [Alvarez-Ramirez et al. \(2019\)](#) have illustrated the high order parametrizations of the stable and unstable manifolds connected with the libration points to allocate the ejection orbits that eject from quadruple collision, in addition, they have also shown the existence of ejection-direct escape orbits analytically.

In the present manuscript we proposed to discuss the motion of the infinitesimal mass, moving in the gravitational influence of the main primaries which are in a syzygy, this setup always referred as collinear restricted four-body problem. In this study we extend the work of authors [Palacios et al. \(2019\)](#) by taking the peripheral primaries as oblate/prolate spheroid.

The present manuscript has following structure: the description of the mathematical model and the equations of motion of the test particle are discussed in Sec. 2. The Sec. 3 deal with the existence of the libration points as function of parameters whereas stability of these libration points is analyzed in the following section. The regions of possible motions are presented in Sec. 5. The BoC linked with the libration points are illustrated in Sec 6. The paper ends with Sec. 7 where the concluding remarks are presented.

## 2 Description of Mathematical model and Equations of motion

The dynamics of the infinitesimal mass (also referred as test particle) moving under the gravitational influence of the three primaries  $P_i, i = 0, 1, 2$  has been investigated in the present problem. It is assumed that the primaries  $P_1$  and  $P_2$ ,

having the same mass  $m_1 = m_2 = m$ , are oblate/prolate bodies and the oblateness/prolateness parameters  $A_1 = A_2 = A$  are also same while the central primary  $P_0$  is spherical in shape. Moreover, we have assumed that the primaries are in collinear central configuration where the primaries  $P_1$  and  $P_2$  are situated symmetrically with respect to the central primary  $P_0$ . Also  $\beta m$ , taken as the mass of the central primary  $P_0$  where  $\beta$  denotes the so called mass parameter, is placed at the center of masses of the system which is taken as origin of the reference frame. The peripheral bodies  $P_{1,2}$  describe the circular orbit around the central primary  $P_0$  with same angular velocity  $\omega$ .

In the synodic frame of reference with the same origin, the line passes through origin and joining the center of mass of  $P_1$  and  $P_2$  is assumed as  $x$ -axis and  $Oy$ -axis is a line perpendicular to  $Ox$ -axis and passing through origin while the line through origin and perpendicular to instantaneous plane of the primaries is assumed as  $Oz$ -axis. Consequently, in the synodic frame of reference, the coordinates of the primaries  $P_i, i = 0, 1, 2$  are  $(x_i, 0, 0)$ ,  $x_0 = 0, x_1 = -x_2 = \frac{1}{2}$ , and  $Gm_0 = \beta$ . The configuration of the primaries remains invariant, if the sum of the total gravitational force exerted by  $P_0$  and  $P_2$  on  $P_1$  are equal to the centrifugal force, i.e.,

$$m_1 \omega^2 \|P_0 P_1\| = \frac{Gm_1 m_0}{\|P_0 P_1\|^2} + \frac{3Gm_0}{2\|P_0 P_1\|^4} I^* + \frac{Gm_1 m_2}{\|P_1 P_2\|^2} + \frac{3Gm_2}{2\|P_1 P_2\|^4} I'^* + \frac{3Gm_1}{2\|P_1 P_2\|^4} I'^*,$$

where

$$I^* = (I_1 + I_2 + I_3 - 3I), \quad I'^* = (I'_1 + I'_2 + I'_3 - 3I'),$$

whereas  $I_i$  and  $I'_i, i = 1, 2, 3$  are the principal moment of inertia of the primaries  $P_1$  and  $P_2$  at its center of mass  $O$ , respectively while  $I$  is the moment of inertia about the line joining the center of mass of the primary  $P_1$  and the primary  $P_0$  or  $P_2$  and  $I'$  is the moment of inertia about the line joining the center of mass of the primary  $P_2$  and the primary  $P_0$  or  $P_1$ . Therefore, the angular velocity of the synodic frame is

$$\omega^2 = \Lambda = 2(1 + 4\beta) + 6A(1 + 8\beta), \quad (1)$$

where  $A_1 = \frac{a_1^2 - c_1^2}{5R^2}, A_2 = \frac{a_2^2 - c_2^2}{5R^2}$  and in the Copenhagen case we have taken  $A_1 = A_2 = A$ . Also, when the oblateness of the primaries are neglected i.e.,  $A = 0$ , the  $\omega^2$  reduces to same as in Eq.(1) in Ref. [Arribas et al. \(2016b\)](#).

The units of distances, mass and time are chosen in such a way that  $\|P_1 P_2\| = 1$ , and  $Gm = 1$ . The equations of motion of the test particle after a change of time  $ds = \omega dt$ , where both of the peripheral bodies are oblate, can be written as:

$$\ddot{x} - 2\dot{y} = \frac{\partial U}{\partial x}, \quad (2a)$$

$$\ddot{y} + 2\dot{x} = \frac{\partial U}{\partial y}, \quad (2b)$$

$$\ddot{z} = \frac{\partial U}{\partial z}, \quad (2c)$$

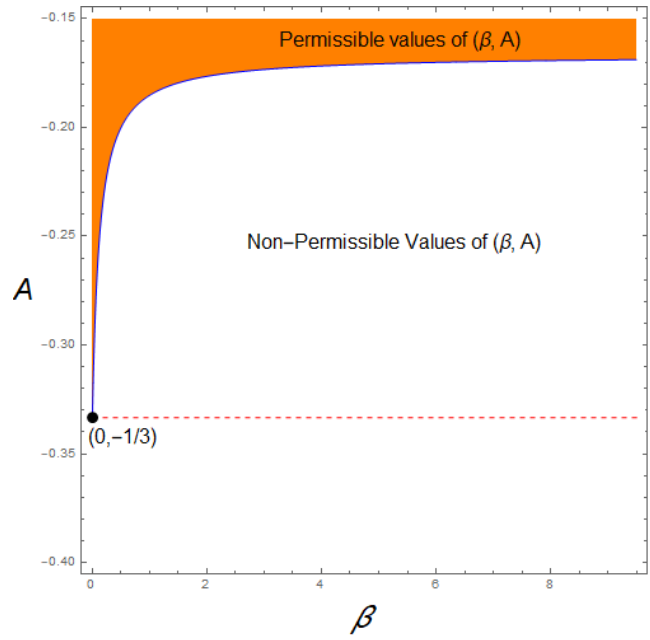


**Fig. 1** The bifurcation curve in the  $(\beta, A)$  plane. (colour figure online).

where

$$U(x, y, z) = \frac{1}{2}(x^2 + y^2) + \frac{1}{\Lambda} \left\{ \frac{\beta}{r_0} + \sum_{i=1}^2 \left( \frac{1}{r_i} + \frac{A_i}{2r_i^3} \right) \right\},$$

$$r_i = \sqrt{(x - x_i)^2 + y^2 + z^2}, \quad i = 0, 1, 2.$$

Furthermore, analogous to the restricted problem of three bodies, the system of equations in Eqs. 2a-2c possesses the first integral, always considered as Jacobi integral, and expressed as

$$C = 2U(x, y, z) - (\dot{x}^2 + \dot{y}^2 + \dot{z}^2), \quad (3)$$

where the Jacobian constant is represented by  $C$ .

### 3 The libration points

The libration points can be obtained by solving the equations

$$U_x = 0, U_y = 0, U_z = 0, \quad (4)$$

where  $U_x, U_y, U_z$  are as follows:

$$U_x = x - \frac{1}{\Lambda} \left\{ \frac{\beta x}{r_0^3} + \sum_{i=1}^2 \tilde{x}_i \left( \frac{1}{r_i^3} + \frac{3A}{2r_i^5} \right) \right\}, \quad (5a)$$

$$U_y = y \left[ 1 - \frac{1}{\Lambda} \left\{ \frac{\beta}{r_0^3} + \sum_{i=1}^2 \left( \frac{1}{r_i^3} + \frac{3A}{2r_i^5} \right) \right\} \right], \quad (5b)$$

$$U_z = -\frac{z}{\Lambda} \left\{ \frac{\beta}{r_0^3} + \sum_{i=1}^2 \left( \frac{1}{r_i^3} + \frac{3A}{2r_i^5} \right) \right\}, \quad (5c)$$

$$\tilde{x}_i = x - x_i. \quad (5d)$$

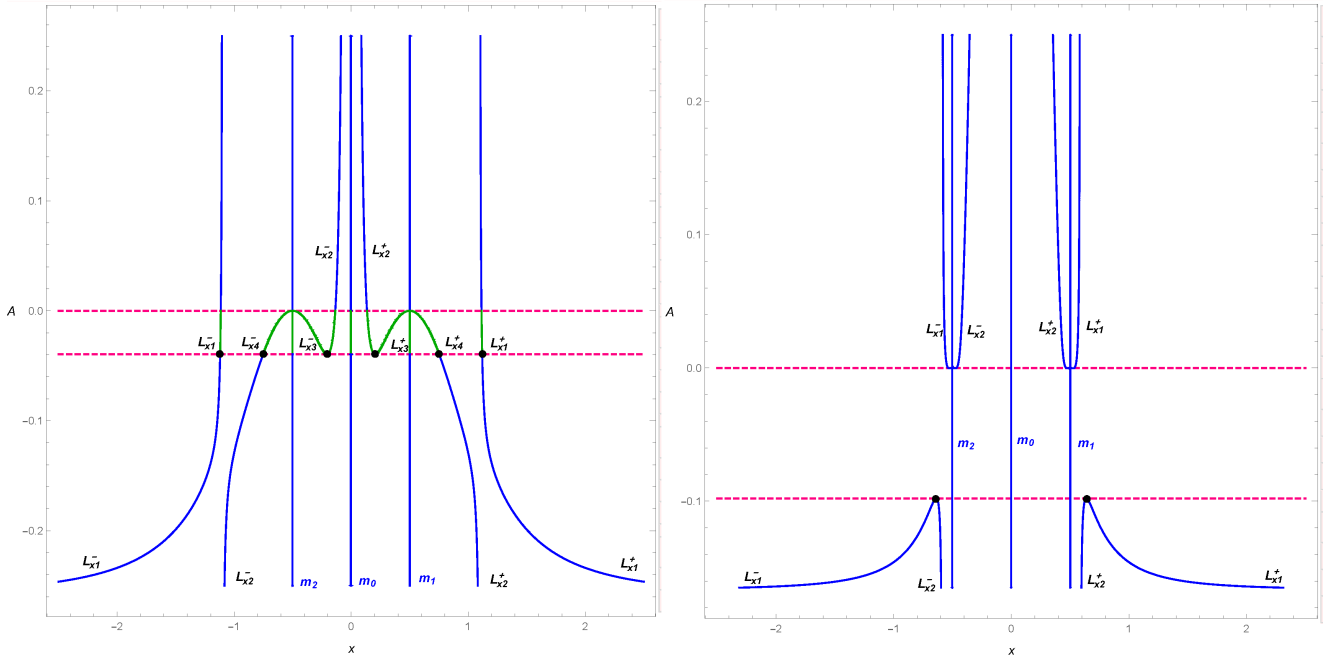


**Fig. 2** Evolution of the positions of collinear libration points  $L_{x1,2,3,4}^+$  and  $L_{x1,2,3,4}^-$  as function of parameter  $A$ ; (a) *left*: for the fixed value of  $\beta = 0.1$ . The horizontal dashed *magenta* lines show the critical value of  $A = 0$  and  $A = -0.039515$ , for this interval of  $A$ , there exist eight collinear libration points. (b) *right*: for  $\beta = 1000$  and the horizontal dashed *magenta* lines show the critical value of  $A = -0.09805989$ , for this interval of  $A \in (-0.166687, -0.09805989)$  and  $(0, 0.25)$ , there exist four collinear libration points whereas in  $A \in (-0.09805989, 0)$  there exist no collinear libration points. (colour figure online).

From the Eq.(1), we observe that  $\Lambda > 0$ , therefore the parameter  $A$  must satisfy the condition  $A > -\frac{(1+4\beta)}{3(1+8\beta)}$ . In Fig. 1, the evolution of the bifurcation curve are presented in the  $(\beta, A)$  plane. In the area below the curve there are non-permissible value of  $(\beta, A)$ , while in the area above the curve there are permissible values of the combination of  $(\beta, A)$ . The red dashed line shows the permissible value of  $A$  when  $\beta = 0$ . It can be observed that for large value of  $\beta$ , the value of  $A$  becomes almost constant, i.e., for  $\beta > 10000$ ,  $A = -0.166669$ .

### 3.1 In plane libration points

The in plane libration points are those libration points which lie on the  $xy$ -plane. When we consider the libration points on the  $xy$ -plane, i.e.,  $z = 0$  and the third equation is always fulfilled. Therefore, the libration points can be found by solving the equations  $U_x = 0$ ,  $U_y = 0$  when  $z = 0$ . There exist two type of libration points in the  $xy$ -plane, i.e., the collinear libration points and the non-collinear libration points.

#### 3.1.1 the collinear libration points

The collinear libration points are solutions of the equation 5a, when  $y = z = 0$ , i.e.,

$$x - \frac{1}{\Lambda} \left[ \frac{\beta x}{|x|^3} + \frac{R^-}{|R^-|^3} + \frac{R^+}{|R^+|^3} + \frac{3A}{2} \left\{ \frac{R^-}{|R^-|^5} + \frac{R^+}{|R^+|^5} \right\} \right] = 0 \quad (6)$$

where,  $x - 1/2 = R^-$  and  $x + 1/2 = R^+$ .

In this subsection, we wish to discuss the effect of oblateness or prolateness, and the mass parameter on the positions of collinear libration points. According to Douskos et al. (2012),  $A < 0$  corresponds to the case of prolate primaries whereas  $A > 0$  corresponds the case of oblate primaries and when  $A = 0$ , the problem converts to the classical case.

The parametric evolution of the positions of collinear libration points are illustrated in Fig. 2 for two different values of  $\beta$ . It is observed that the positions as well as the number of libration points on  $x$ -axis strongly depend on the combination of the values of  $\beta$  and  $A$ . For  $\beta = 0.1$ , there exist 8 collinear libration points for  $A \in (-0.039515, 0)$  whereas there exist only 4 libration points for  $A \in [0, 1)$  and  $A \in [-0.259259, -0.039515)$ . The libration points  $L_{x3,4}^+$  and  $L_{x3,4}^-$  originate from the vicinity of the primaries  $m_1$  and  $m_2$  respectively for slightly negative value of  $A$ , and  $L_{x3}^+$ ,  $L_{x3}^-$  coincide with  $L_{x2}^+$ ,  $L_{x2}^-$  respectively and disappear completely at  $A = -0.039515$  whereas  $L_{x4}^+$ ,  $L_{x4}^-$  exist for  $A < -0.039515$

which we again labeled as  $L_{x2}^+$ ,  $L_{x2}^-$  for  $A \in [-0.259259, -0.039515]$ . In addition, when  $\beta = 1000$ , there exist 4 collinear libration points for  $A \in (-0.166687, -0.09805989)$  and  $A \in (0, 1)$  whereas there exist no collinear libration point when  $A \in (-0.09805989, 0)$ . In addition, we can notice that there originate a pair of collinear libration points in the vicinity of the each peripheral primaries, i.e., there exist four collinear libration points in total.

### 3.1.2 the non-collinear libration points

The non-collinear libration are solutions of Eqs (5a, 5b) when  $y \neq 0$ . In this subsection, we discuss the locations of the libration points evaluated numerically, by well known Newton-Raphson iterative scheme. This method operates good concerning the convergence and the reliability of the results for the particular class of equations and this is exactly the reason why we have used this method. It is necessary to note that the Newton-Raphson method behaves well on the proper choice of the initial condition and consequently, for the good choice of initial conditions, we have used the efficient and smart technique introduced by [Arribas et al. \(2016a\)](#).

In Fig. 3, the parametric evolution of the positions of libration points on the  $(x, y)$ -plane are illustrated for the different values of  $\beta$  and  $A$ . In Fig. 3(a-c), the value of  $\beta = 0.1$  is fixed and values of  $A$  decreases. It is observed that there exist 14 libration points in which four libration points originate in the vicinity of the each of peripheral primaries. As the value of  $A$  decreases, the libration points  $L_{x3}^+$ ,  $L_{x4}^+$  and  $L_{x3}^-$ ,  $L_{x4}^-$  move towards each other and collide and finally disappear completely (see Fig. 3b). Further decrease in the value of  $A$  leads to the result that the libration points  $L_{xy1,2}^+$  and  $L_{xy1,2}^-$  disappear completely (see Fig. 3c) and consequently there exist the libration points which lie only on the axes.

In Fig. 3(d-e), we have illustrated the in-plane libration points for the value of  $\beta = 1000$  and observe completely different results regarding the existence and movement of the libration points. This clearly indicates that the existence and the movement of the libration points depend on both the parameters, i.e.,  $\beta$  and  $A$ . It is observed that the libration points  $L_{x1}^+$ ,  $L_{x2}^+$  and  $L_{x1}^-$ ,  $L_{x2}^-$  move towards each other and disappear completely as the value of  $A$  increases and consequently there exists no libration point on the  $x$ -axis (see Fig. 3f).

In Fig. 4, we have illustrated the parametric evolution of the positions of the libration points for varying value of the oblateness/prolateness parameter and fixed value of the mass parameter  $\beta = 0.1$ . It can be observed that, for slightly higher value of the prolateness parameter  $A$ , there exist four collinear libration points whereas in the vicinity of libration points  $L_{x2}^\pm$  there originate a pair of non-collinear libration points  $L_{xy1,xy2}^\pm$  which first move away from  $x$ -axis as the value of  $A$  increases i.e., when  $A \in (-0.259259, \mathbf{B})$ , four

collinear libration points exist in which two libration points lie on  $y$ -axis and four libration points lie on the  $xy$ -plane. The collinear libration points  $L_{x1}^\pm$  and  $L_{x2}^\pm$  move towards the peripheral primaries, the libration points  $L_{y1}^\pm$  move towards the central primary whereas the non-collinear libration points  $L_{xy1}^\pm$  and  $L_{xy2}^\pm$  move far from the  $x$ -axis first then again turn towards the  $x$ -axis as  $A \in (-0.259259, \mathbf{B})$  and finally annihilate in the vicinity of the peripheral primaries as  $A \in (\mathbf{B}, \mathbf{C})$ . Further, when  $A \in (\mathbf{B}, \mathbf{C})$  we can observe that there exist eight collinear libration points in total and two new collinear libration points  $L_{x3}^\pm$  and  $L_{x4}^\pm$  originate in which the libration points  $L_{x3}^\pm$  move towards peripheral primaries and at  $A = 0$  these libration points annihilate in the vicinity of them respectively, and the libration points  $L_{x4}^\pm$  move towards the central primary as the value of parameter  $A$  increases and the movement of the remaining libration points are same. Further, when  $A > 0$ , there exists no libration point on the  $xy$ - plane, on the contrary the libration points always exist on either of the axes (shown in blue colour line). It can be observed that the libration points  $L_{x1}^\pm$  and  $L_{y1}^\pm$  move towards the central primary  $m_0$  along the  $x$ -axis and  $y$ -axis respectively.

In Fig. 5, we have illustrated the parametric evolution of the positions of libration points for the fixed value of  $\beta = 1000$  and varying values of  $A \in (-0.166687, 1)$ . The *magenta, cyan, olive and orange* dots represented by **A**, **B**, **C**, and **D** respectively show the critical values of the oblateness/prolateness parameters where the number of libration points changes. It is observed that as the value of  $A$  is slightly greater than the permissible value i.e.,  $-0.166687$ , six libration points exist in which four libration points namely  $L_{x1,x2}^+$  and  $L_{x1,x2}^-$  exist on  $x$ -axis and two libration points  $L_{y1}^+$ ,  $L_{y1}^-$  exist on  $y$ -axis. As the value of  $A$  approaches to **A** (shown by magenta dots in Fig. 5), four non-collinear libration points namely  $L_{xy1}^+$ ,  $L_{xy1}^-$  and  $L_{xy2}^+$ ,  $L_{xy2}^-$  originate in the vicinity of the collinear libration points  $L_{x1}^+$  and  $L_{x1}^-$  respectively, and it can be further observed that these libration points move away from the  $x$ -axis whereas the collinear libration points  $L_{x1}^\pm$  move towards and  $L_{x2}^\pm$  move away from the peripheral primaries as value of  $A$  increases. In addition, at **B** (shown by cyan dot) the collinear libration points  $L_{x1}^\pm$  collide with  $L_{x2}^\pm$  respectively, and disappear. Consequently, there exists no collinear libration point for prolateness parameter  $A \in (\mathbf{B}, \mathbf{C})$  (shown in darker blue line) and only the non-collinear libration points  $L_{xy1,2}^\pm$  and  $L_{y1}^\pm$  exist in this range and at **C**, the non-collinear libration points  $L_{xy1,2}^\pm$  collide with the peripheral primaries and disappear completely. Further, when  $A \in (\mathbf{C}, 0.25)$ , a pair of collinear libration points originate in the vicinity of each of the peripheral primaries and move far from them as the value of  $A$  increases (shown in darker gray line). In this interval, for the values of the oblateness parameter, there exist six libration points in total which lie on either of the axes (shown in darker gray

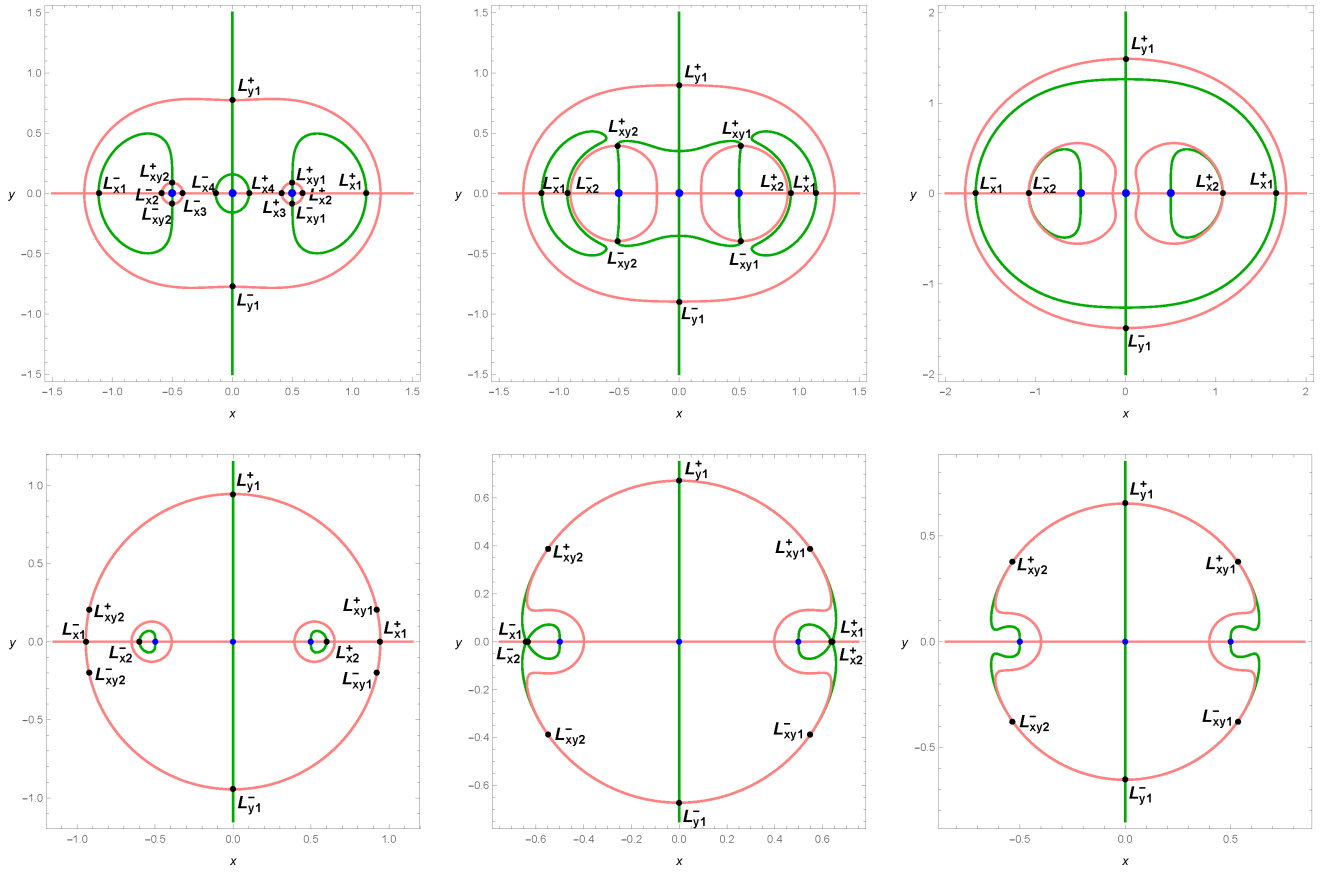


**Fig. 3** The evolution of the positions of the libration points, *first row*: for  $\beta = 0.1$  : (a) left:  $A = -0.005$ ; (b) middle:  $A = -0.1$ ; (c) right:  $A = -0.215$ ; *second row*: for  $\beta = 1000$  : (d) left:  $A = -0.142$ ; (e) middle:  $A = -0.09804989$ ; (f) right:  $A = -0.092$ . The blue dots show the positions of primaries. (colour figure online).

line). It is noticed that as the value of oblateness/prolateness parameter  $A$  increases the libration points  $L_{y1}^{\pm}$  always move towards the origin along  $y$ -axis.

#### 4 The Stability of libration points

In this section, we deal with the stability of the libration points in the configuration  $(x, y)$ -plane, where the effects of the parameters  $A$  and  $\beta$  on the stability of these libration points are illustrated. The stability of the libration points can be determined by linearizing the equations of motion of the test particle given in Eqs. 2a-2b about the libration point  $(x_*, y_*)$ . Consequently, the linearized equations for the test particle near the libration points in the collinear restricted four-body problem are  $\dot{\mathbf{x}} = \mathbf{A}\mathbf{x}$ , where  $\mathbf{x} = (x, y, \dot{x}, \dot{y})^T$ , and  $\mathbf{x}$  is the state vector of the infinitesimal body with respect to the libration points and  $\mathbf{A}$ , the coefficient matrix is read as:

$$\mathbf{A} = \begin{pmatrix} \mathbf{O} & \mathbf{I} \\ \mathbf{B} & \mathbf{C} \end{pmatrix}, \quad (7)$$

where

$$\mathbf{O} = \begin{pmatrix} 0 & 0 \\ 0 & 0 \end{pmatrix}, \mathbf{I} = \begin{pmatrix} 1 & 0 \\ 0 & 1 \end{pmatrix},$$

$$\mathbf{B} = \begin{pmatrix} A_{11} & A_{12} \\ A_{21} & A_{22} \end{pmatrix}, \mathbf{C} = \begin{pmatrix} 0 & 2 \\ -2 & 0 \end{pmatrix}.$$

Accordingly, the characteristic equation corresponding to the matrix given in Eq. 7 is

$$\lambda^4 + a_1\lambda^2 + a_0 = 0, \quad (8)$$

where

$$a_1 = 4 - A_{11} - A_{22},$$

$$a_0 = A_{11}A_{22} - A_{12}^2,$$

$$A_{11} = 1 - \frac{1}{\Lambda} \left( \frac{\beta}{r_0^3} + \sum_{i=1}^2 \left( \frac{1}{r_i^3} + \frac{3A}{2r_i^5} \right) \right) + \frac{1}{\Lambda} \left( \frac{3\beta x_*^2}{r_0^5} \right.$$

$$\left. + \sum_{i=1}^2 \tilde{x}_i^2 \left( \frac{3}{r_i^5} + \frac{15A}{2r_i^7} \right) \right),$$

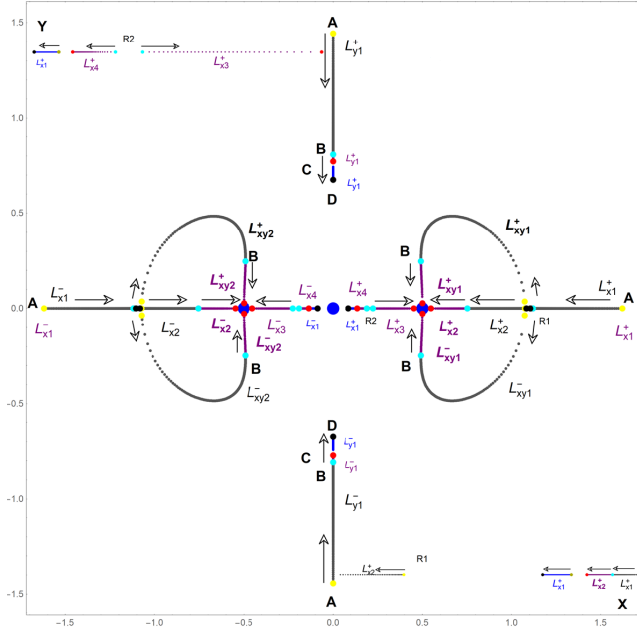


**Fig. 4** The movement of the positions of the libration points on  $(x, y)$ -plane for  $\beta = 0.1$  and  $A \in (-0.259259, 0.25)$ , the yellow dots show the value of the parameter  $A = \mathbf{A} \approx -0.259259$ , the cyan dots show the value of  $A = \mathbf{B} = -0.039515$ , the red dots show the value of  $A = \mathbf{C} = 0$ , and the black dots show the value of  $A = \mathbf{D} = 0.25$ . The arrow represents the movement of the positions of libration points while the big blue dots show the positions of primaries. (colour figure online).

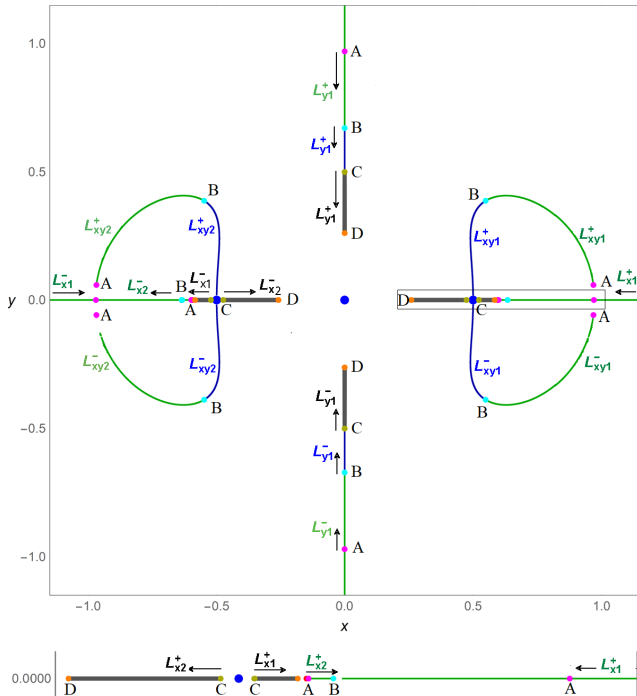


**Fig. 5** The movement of the positions of the libration points for  $\beta = 1000$  and the parameter  $A \in (-0.166687, 1)$ . The magenta dots show the value of parameter  $A = \mathbf{A}$ , cyan dots show the value of  $A = \mathbf{B} = -0.097968$ , orange dots show the value of  $A = \mathbf{C} = 0$ , and blue dots show the value of  $A = \mathbf{D} \approx 1$ . The arrow shows the movement of the positions of libration points. The big blue dots show the positions of the primaries. (colour figure online).

$$A_{22} = 1 - \frac{1}{\Lambda} \left( \frac{\beta}{r_0^3} + \sum_{i=1}^2 \left( \frac{1}{r_i^3} + \frac{3A}{2r_i^5} \right) \right) + \frac{y_*^2}{\Lambda} \left( \frac{3\beta}{r_0^5} + \sum_{i=1}^2 \left( \frac{3}{r_i^5} + \frac{15A}{2r_i^7} \right) \right),$$

$$A_{12} = \frac{y_*}{\Lambda} \left( \frac{3\beta x_*}{r_0^5} + \sum_{i=1}^2 \tilde{x}_i \left( \frac{3}{r_i^5} + \frac{15A}{2r_i^7} \right) \right),$$

$$= A_{21}.$$

$$\tilde{x}_i = x_* - x_i,$$

$$r_i = \sqrt{(x_* - x_i)^2 + y_0^2}, i = 0, 1, 2.$$

A libration point is said to be stable if the solution of the Eq.8, evaluated at the libration point, has four pure imaginary roots. This is true only when the conditions,

$$a_1^2 - 4a_0 > 0, \quad a_1 > 0, \quad a_0 > 0, \quad (9)$$

are satisfied simultaneously.

In Fig. 6, we have illustrated the linear stability of the collinear equilibrium points. In Fig. 6a and Fig. 6b, the stability of the equilibrium points are depicted for constant value of  $\beta = 0.0001$  and  $\beta = 5$  respectively. In both the cases, we observed that equilibrium points  $L_{x2}^{\pm}$  and  $L_{x3}^{\pm}$  are stable. However, as the value of  $\beta$  increases, the intervals of the values of parameter  $A$  decreases in which the libration points are stable. In Fig. 6c, the stability of collinear libration points are presented for fixed value of  $A = -0.02$  and varying values of  $\beta$  and observed that  $L_{x2}^{\pm}$  and  $L_{x3}^{\pm}$  are stable for  $\beta \in (0, 2.29207325)$  and  $\beta \in (0, 0.63939639)$  respectively.

In Fig. 7, the stability of the libration points for  $\beta = 0.1$  and 1000 is presented for varying values of the parameter  $A$ . In Fig. 7a, the stability of the libration points is presented for mass parameter  $\beta = 0.1$ . It is unveiled that the libration points  $L_{x2}^{\pm}$  are linearly stable for  $A \in (\mathbf{A}, \mathbf{B})$  and  $A \in (\mathbf{B}, \mathbf{C})$  (the stable equilibrium points are depicted in thick orange and green lines respectively). Further, the equilibrium points  $L_{x3}^{\pm}$  are linearly stable for  $A \in (\mathbf{B}, \mathbf{C})$ .

In Fig. 7b, the stability of the libration points is presented for  $\beta = 1000$  and we noticed that the collinear libration points  $L_{x2}^{\pm}$  are stable for  $A \in (\mathbf{A}, \mathbf{B})$  whereas  $L_{y1}^{\pm}$  are also stable for  $A \in (\mathbf{A}, \mathbf{B})$ . In addition, we have observed that the  $L_{y1}^{\pm}$  are stable for the value of  $A \in (\mathbf{B}, \mathbf{C})$  and  $A \in (\mathbf{C}, 1)$  also. It is also observed that none of the libration points which lie on  $(x, y)$  plane are stable, however, for some mass ratio the equilibrium points which lie on  $y$ -axis are linearly stable.

## 5 The regions of possible motion

By using the relation 3, we shall draw the evolution of the zero-velocity curves for fixed value of  $C$ , by assuming the motions of the particle on the  $xy$ -plane. The zero-velocity curves bifurcate the regions of possible motion of those planes

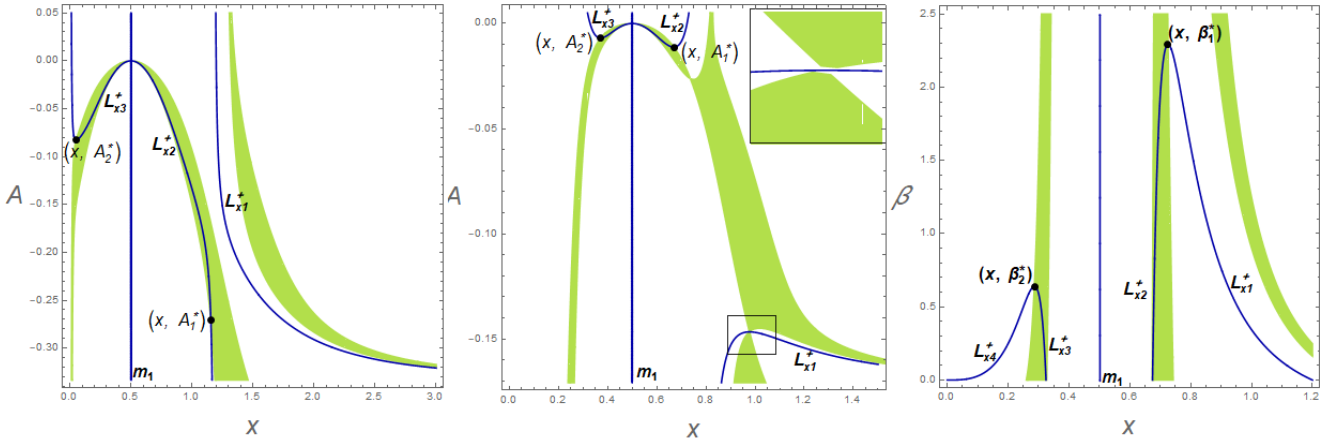


**Fig. 6** The parametric evolution of the stability of collinear libration points: (a) *left*: for  $\beta = 0.0001$  and  $(x, A_1^*) = (1.15454220, -0.27055522)$ , and  $(x, A_2^*) = (0.05161635, -0.08262583)$ ; (b) *middle*: for  $\beta = 5$  and  $(x, A_1^*) = (0.66910678, -0.01123429)$ , and  $(x, A_2^*) = (0.37141443, -0.00690825)$ ; (c) *right*: for  $A = -0.02$  and  $(x, \beta_1^*) = (0.72564641, 2.29207325)$ , and  $(x, \beta_2^*) = (0.28636778, 0.63939639)$ . The stable regions are depicted by *green* colour. (colour figure online).

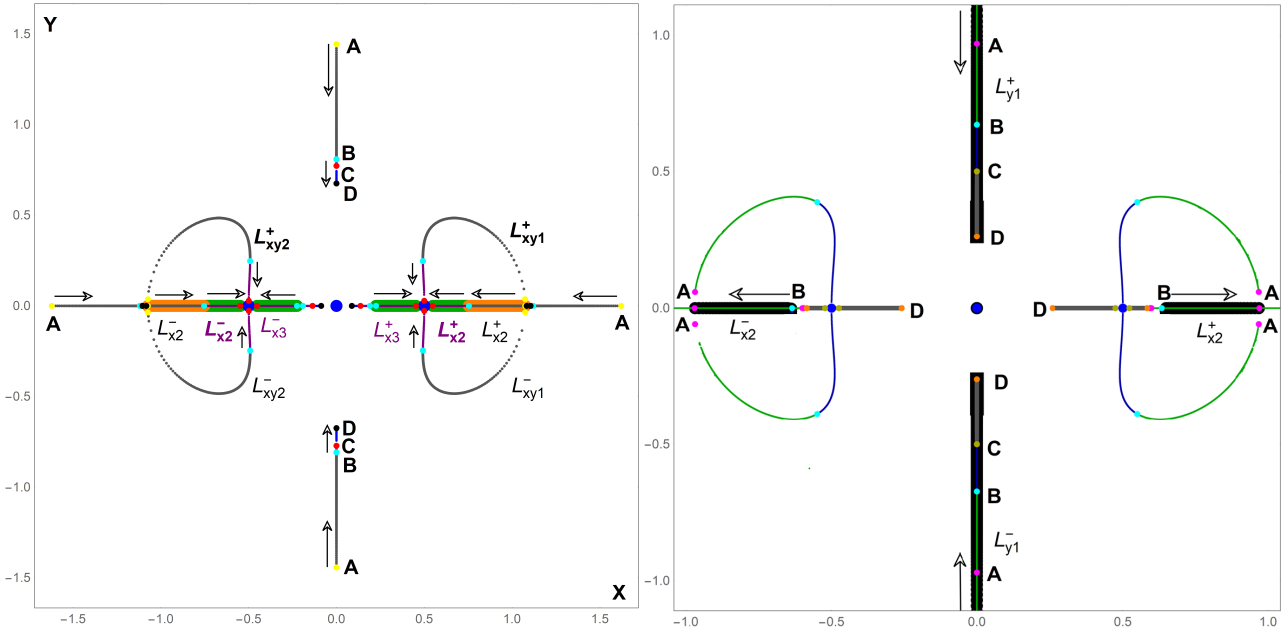


**Fig. 7** The parametric evolution of the stability regions of the libration points for (a) *left*:  $\beta = 0.1$  and  $A \in (-0.259259, 0.25)$ , here the thick orange and green lines show the positions of the stable libration points. The value of **A**, **B**, **C**, and **D** are same as in Fig. 4; (b) *right*:  $\beta = 1000$  and  $A \in (-0.166687, 1)$ , thick black lines show the positions of stable libration points. The values of **A**, **B**, **C**, and **D** are same as in Fig. 5. (colour figure online).

from the forbidden region where the test particle can not orbit.

In Fig. 8(a, b, c), the regions of possible motion are depicted for the fixed value of  $\beta$ , the prolateness parameter  $A$  and increasing value of the Jacobian constant  $C$ . The coloured area represents the forbidden regions where the test particle can not communicate. At  $C = C_{L_{y1}^+} = C_{L_{y1}^-}$ , there exist two circular islands containing each of the peripheral primaries where the motion of the test particle is not possible. Therefore, the test particle can orbit from central primary to any libration points whereas it can not orbit to peripheral

primaries. In 8b, when the Jacobian constant  $C$  is increased to  $C = C_{L_{x1}^+} = C_{L_{x1}^-}$  the forbidden region increased and two crescent shapes appear which originate from  $L_{x1}^+$  or  $L_{x1}^-$  and contain the libration points  $L_{y1}^+$  or  $L_{y1}^-$ , respectively. Consequently, the infinitesimal mass cannot approach to these libration points. Further increase in value of Jacobian constant to  $C = C_{L_{x2}^+} = C_{L_{x2}^-}$  leads to further increase in the forbidden regions and consequently all the libration points fall inside the forbidden region. The test particle can move either outside the circular annulus shaped region or in the vicinity of the central primary. Therefore, we can conjuncture that as



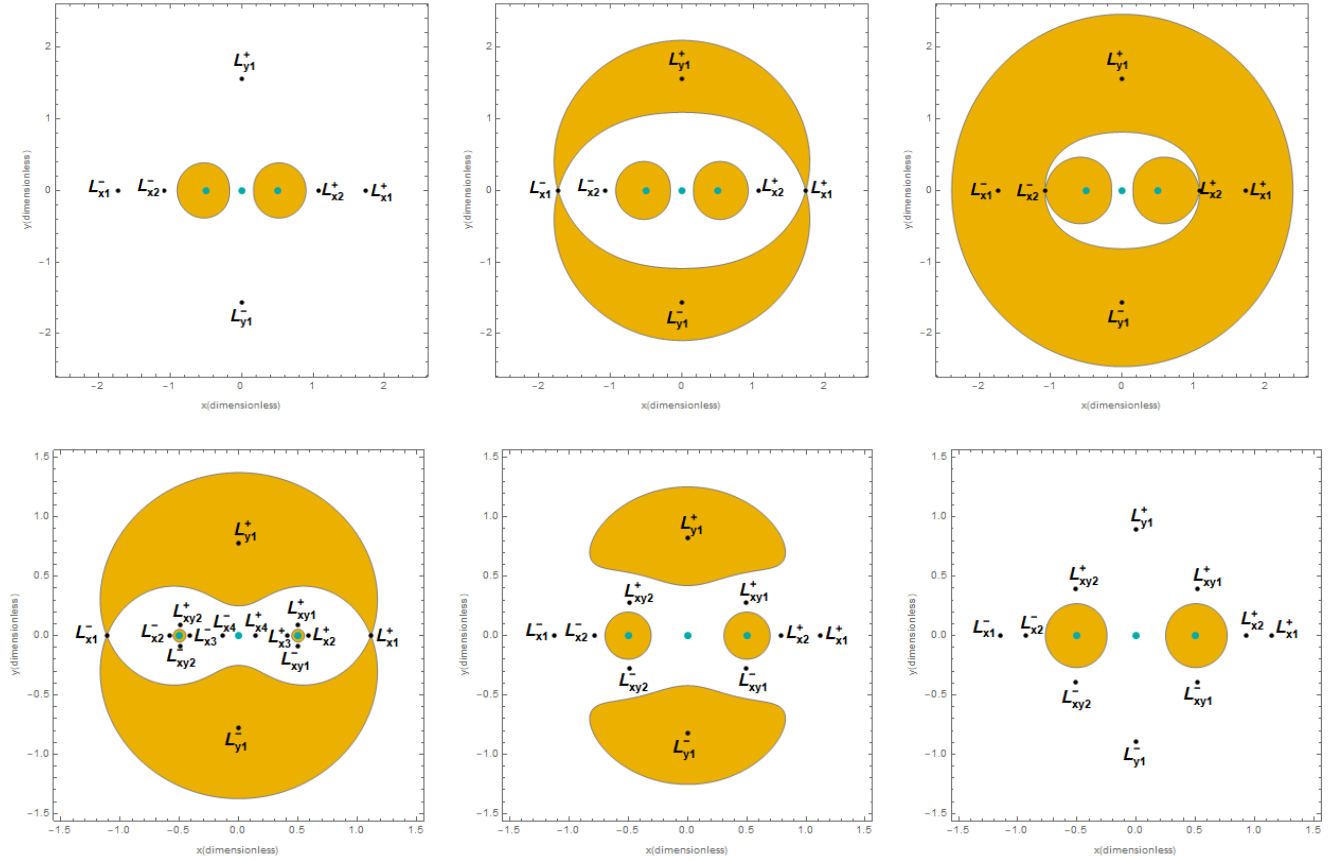


**Fig. 8** The evolution of the regions of possible motion: *first row*: for  $\beta = 0.1, A = -0.22$ : (a) left:  $C = 8.25875064$ ; (b) middle:  $C = 8.89008187$ ; (c) right:  $C = 9.93069941$ .; *second row*: for  $C = 2.93554384$ , (a) left:  $A = -0.005$ , (b) middle:  $A = -0.05$ , (c) right:  $A = -0.1$ . (colour figure online).

the value of Jacobian constant increases, the forbidden region also increases.

In Fig. 8(d, e, f), the ZVCs are depicted for the fixed values of  $\beta, C$  and the varying values of prolateness parameter  $A$ . It can be noticed that when  $A = -0.005$ , there exist four branches of forbidden regions, in which two are circular in shaped which contain the peripheral primaries whereas two crescent shaped regions contain the libration points which exist on  $y$ -axis. However, the motion of the infinitesimal mass is possible inside the pear shaped region which contains all the libration points except those which lie on the  $y$ - axis. As we decrease the value of parameter  $A = -0.05$ , the crescent shape regions containing libration points  $L_{y1}^+$  and  $L_{y1}^-$  shrink and further shrink to libration points  $L_{y1}^+$  and  $L_{y1}^-$  as the value of  $A$  approaches to  $\approx -0.08741$ . It is observed that the circular shaped forbidden regions containing the peripheral primaries do exist even for higher values of  $A$ . Consequently, the test particle can not communicate from peripheral primaries to any other and vice-versa.

In Fig. 9(a-f), the regions of possible motion are depicted for fixed value of the parameters  $A$  and  $\beta$  and increasing values of the Jacobian constant. It is observed that the regions

of possible motion decrease significantly when the value of the Jacobian constant increases.

## 6 The basins of convergence

In the present manuscript a systematic study related to the basins of convergence (BoC) associated with the libration points are presented when the peripheral primaries are non-spherical in shape. The well known method in multivariate version, i.e., Newton-Raphson method is used to solve the nonlinear equations. In addition, we will use the procedure and methodology used by Zotos (2016) to illustrate the domain of the basins of convergence in the in-plane case only.

The associated multivariate iterative scheme is

$$\mathbf{x}_{n+1} = \mathbf{x}_n - \mathbb{J}^{-1} f(\mathbf{x}_n), \quad (10)$$

where  $f(\mathbf{x}_n)$  shows the system of equations, whereas the associated inverse Jacobian matrix is given by  $\mathbb{J}^{-1}$ . In our system 2a-2c, we have three equations.

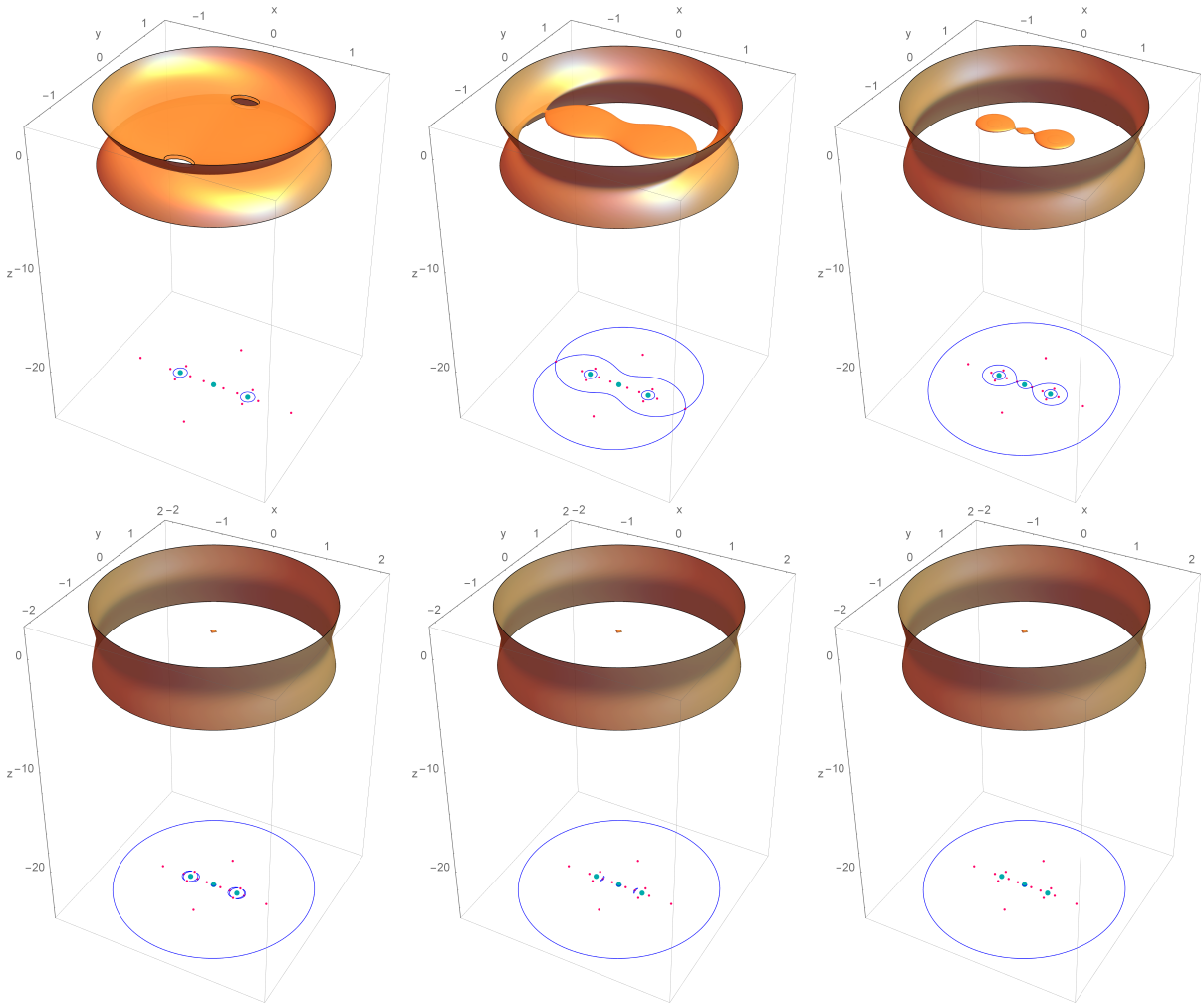


**Fig. 9** The evolution of the regions of possible motion when  $A = -0.015$ ;  $\beta = 0.1$ : (a) top left:  $C = 2.32787248$ ; (b) top middle:  $C = 2.98763159$ ; (c) top right:  $C = 3.70660029$ ; (d) bottom left:  $C = 4.53152976$ ; (e) bottom middle:  $C = 4.56457186$ ; (f) bottom right:  $C = 4.59237937$ . (colour figure online).

Thus, we can use the multivariate NR iterative scheme on the system:

$$U_x(x, y) = 0, \quad (11a)$$

$$U_y(x, y) = 0, \quad (11b)$$

and for the configuration  $(x, y)$  plane, for each coordinate, the bivariate version of the iterative scheme are read as:

$$x_{n+1} = x_n - \frac{U_{x_n} U_{y_n y_n} - U_{y_n} U_{x_n y_n}}{U_{x_n x_n} U_{y_n y_n} - U_{x_n y_n} U_{y_n x_n}}, \quad (12a)$$

$$y_{n+1} = y_n + \frac{U_{x_n} U_{y_n x_n} - U_{y_n} U_{x_n x_n}}{U_{x_n x_n} U_{y_n y_n} - U_{x_n y_n} U_{y_n x_n}}. \quad (12b)$$

In the above equations, the values of  $x$  and  $y$  coordinates at the  $n$ -th step of the iterative scheme are given by  $x_n$  and  $y_n$  in the Newton-Raphson method. Here, the corresponding second order partial derivatives of the potential function are represented by the subscripts of  $U(x, y)$ .

The philosophy that works behind the Newton-Raphson iterative scheme is as follows: the numerical code activates

when the initial condition  $(x_0, y_0)$  is provided on the plane, whereas the iterative scheme continues until an attractor (i.e., equilibrium point) is achieved, with the coveted predefined accuracy. Whenever the specific initial condition reached to one of the attractor (i.e., libration point) of the dynamical system, we claim that for that specific initial condition, the iterative scheme converges. It can be noted that the iterative scheme does not converge equally well for each of the initial conditions, in general. The collections of all those initial conditions which converge to the same attractor compile the so-called BoC or NR basins of attraction.

It is well known that in the dynamical system such as  $N$ -body problem, it is not always possible to find the analytic formulae to evaluate the coordinates of positions of the equilibrium points. In fact, for  $N > 3$ , we do not have any analytical formulae to evaluate the position of the libration point, thus, the one of the best means is to use the numerical methods to evaluate their positions numerically. At this point

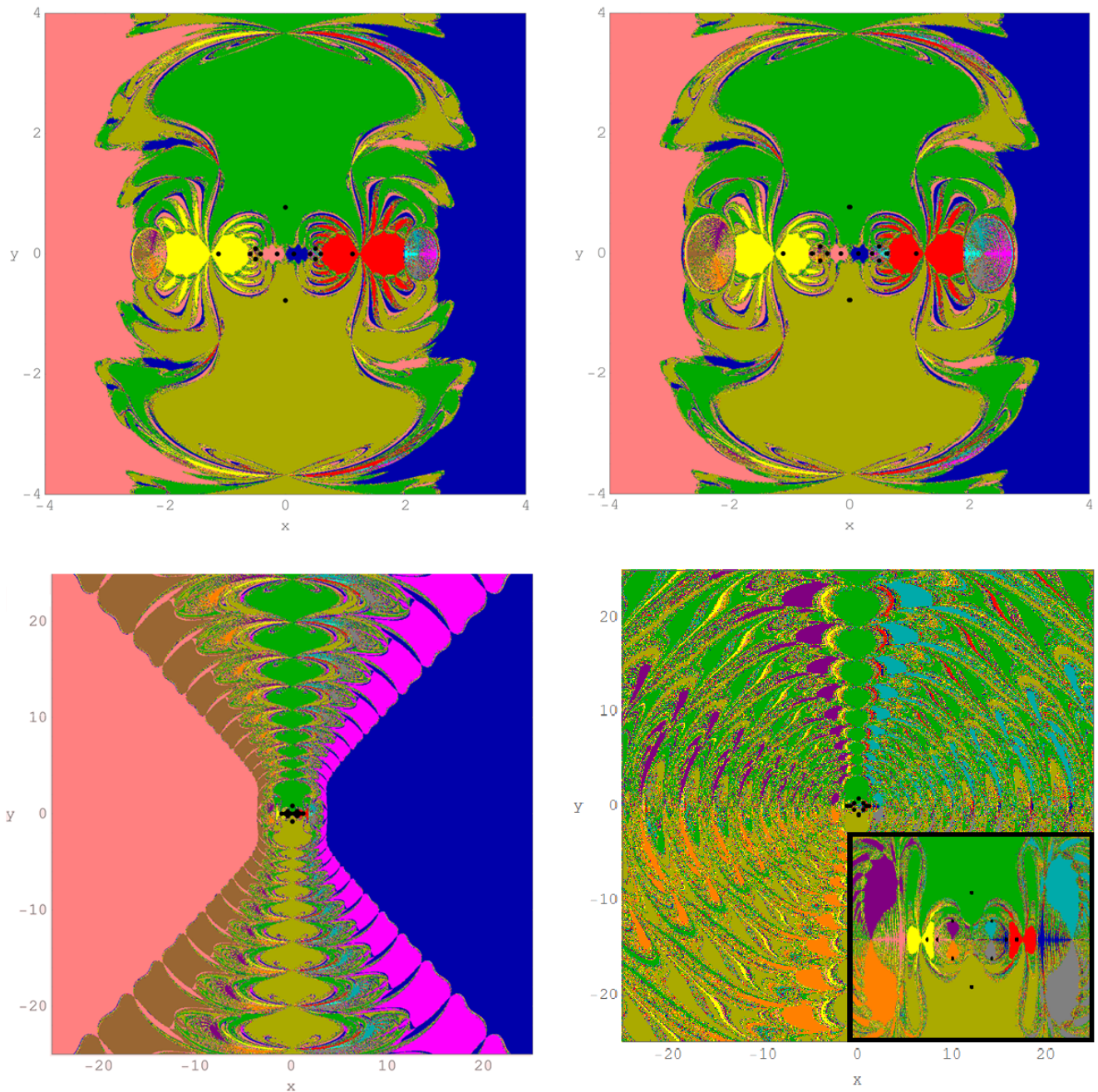


**Fig. 10** The BoC linked with the libration points on  $(x,y)$ -plane for  $\beta = 0.1$ , and for (a)  $A = -0.005$ , (b)  $A = -0.01$ , (c)  $A = -0.0391$ , (d)  $A = -0.075$ . The color codes for the BoC are as follows:  $L_{x1}^+ = \text{red}$ ,  $L_{x2}^+ = \text{cyan}$ ,  $L_{x3}^+ = \text{magenta}$ ,  $L_{x4}^+ = \text{blue}$ ,  $L_{x1}^- = \text{yellow}$ ,  $L_{x2}^- = \text{light pink}$ ,  $L_{x3}^- = \text{brown}$ ,  $L_{x4}^- = \text{pink}$ ,  $L_{y1}^+ = \text{green}$ ,  $L_{y1}^- = \text{olive}$ ,  $L_{xy1}^+ = \text{teal}$ ,  $L_{xy2}^+ = \text{purple}$ ,  $L_{xy1}^- = \text{gray}$  and  $L_{xy2}^- = \text{orange}$ . The dots show the positions of libration points. (colour figure online).

of time it is necessary to note that every numerical method strongly depends on the choice of initial conditions. Indeed, the numerical methods may converge to one of the attractors (i.e., the roots) or may need a vast number of iteration for some of the initial conditions to converge at one of the attractor while for some of the initial conditions the numerical method may trapped into an endless cycle in a periodic or aperiodic manner or may diverge to infinity. This fact leads

to the conclusion that the choice of initial condition must be good so that the method may converge to one of the attractor. The various literature concerning the iterative scheme suggest that those initial conditions need less number of the iterations which lie in the regular domain of the basins of convergence, on the other hand the initial conditions which fall in the fractal region may need a huge number of iterations to converge at one of the attractor. The above mentioned facts

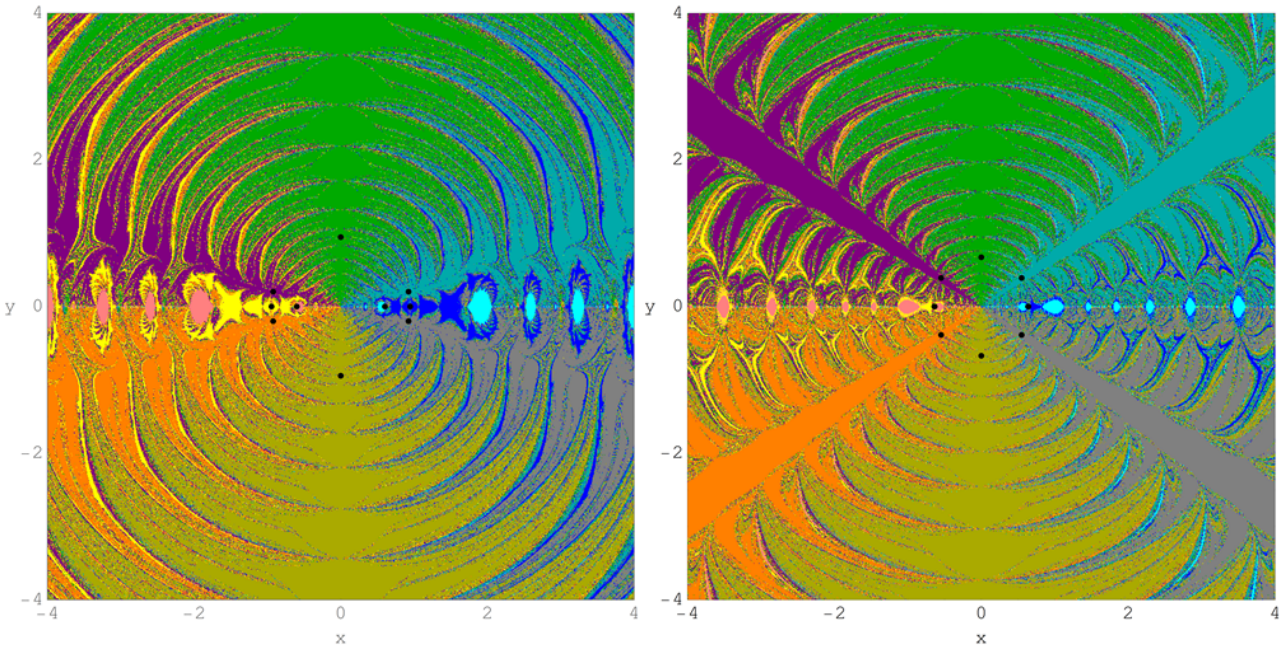


**Fig. 11** The BoC linked with the libration points on  $(x,y)$ -plane for  $\beta = 1000$ , and (a) for  $A = -0.142$ , (b)  $A = -0.09804989$ . The color codes for the BoC are as follows:  $L_{x1}^+ = \text{blue}$ ,  $L_{x2}^+ = \text{cyan}$ ,  $L_{x1}^- = \text{yellow}$ ,  $L_{x2}^- = \text{pink}$ ,  $L_{y1}^+ = \text{green}$  and  $L_{y1}^- = \text{olive}$ ,  $L_{xy1}^+ = \text{teal}$ ,  $L_{xy2}^+ = \text{purple}$ ,  $L_{xy1}^- = \text{gray}$ ,  $L_{xy2}^- = \text{orange}$ . The dots show the positions of libration points. (colour figure online).

give us a considerable amount of reason to examine the BoC corresponding to the equilibrium points. Consequently, we can pick those initial conditions easily for which the iterative method need lowest number of iterations to converge at one of the specific attractor with predefined accuracy. Moreover, the most intrinsic properties of the dynamical system are unveiled by the analysis of the BoC corresponding to the libration points. Since , the equations (12a, 12b) contain the first and second order derivatives which combine the dynamics of the test particle's orbit together with the corresponding stability properties and therefore, it gives a strong reason for revealing the basins of attraction in the present dynamical model.

Recently, various scientists and researchers have deplete their time to analyze the NRBoC in different types of dynamical systems, such as the restricted problem of three bodies (e.g., Douskos (2010), Zotos (2016), Zotos (2017a)), the restricted problem of four bodies (e.g., Zotos (2016), Suraj et al. (2017a), Suraj et al. (2017b)), and the restricted problem of five bodies (e.g., Zotos and Suraj (2017)).

To illustrate the NRBoC, we deploy the following algorithm: we classify the configuration plane into dense uniform grids of  $1024 \times 1024$  initial conditions  $(x_0, y_0)$  and perform a double scan of the configuration  $(x,y)$  plane. For the present numerical computations, the maximum number  $N_{max}$  of iterations allowed is set to 500 while the predefined accuracy is set to  $10^{-15}$  regarding the coordinates of the equilibrium points. At this point of time it is necessary to make clear that the Newton-Raphson BoC must not be

mistaken with the basins of attraction of that of dissipative systems. It should be noted that the present manuscript deals with numerical attractors and the BoC associated with them.

## 6.1 In-plane basins of convergence

We begin our numerical analysis with the in-plane case i.e., for the case when libration points lie on  $(x,y)$  plane only. To classify each nodes on the configuration plane we have used the color coded diagrams (CCDs), where each different color is associated with each pixel, as per the final stage of the associated initial conditions. In Section 3, we have illustrated that there exist different type of sets of libration points for different combinations of the parameter  $\beta$  and  $A$ . On this basis we have divided our analysis in following subsections.

### 6.1.1 When libration points lie on $xy$ -plane

In this subsection, we have discussed the BoC in those cases for which the libration points exist on the axes as well as on the  $xy$ -plane. In Fig.10, we have illustrated the BoC for fixed value of  $\beta = 0.1$  and various values of parameter  $A$ . The configuration plane is covered by well formed BoC linked to the equilibrium points. Moreover, the extent of BoC are infinite linked to all libration points. We observed that the libration points linked to  $L_{x1}^-$  and  $L_{x1}^+$  are resemble with exotic bugs with many legs and antennas. It is obvious that the majority of area of the configuration plane are

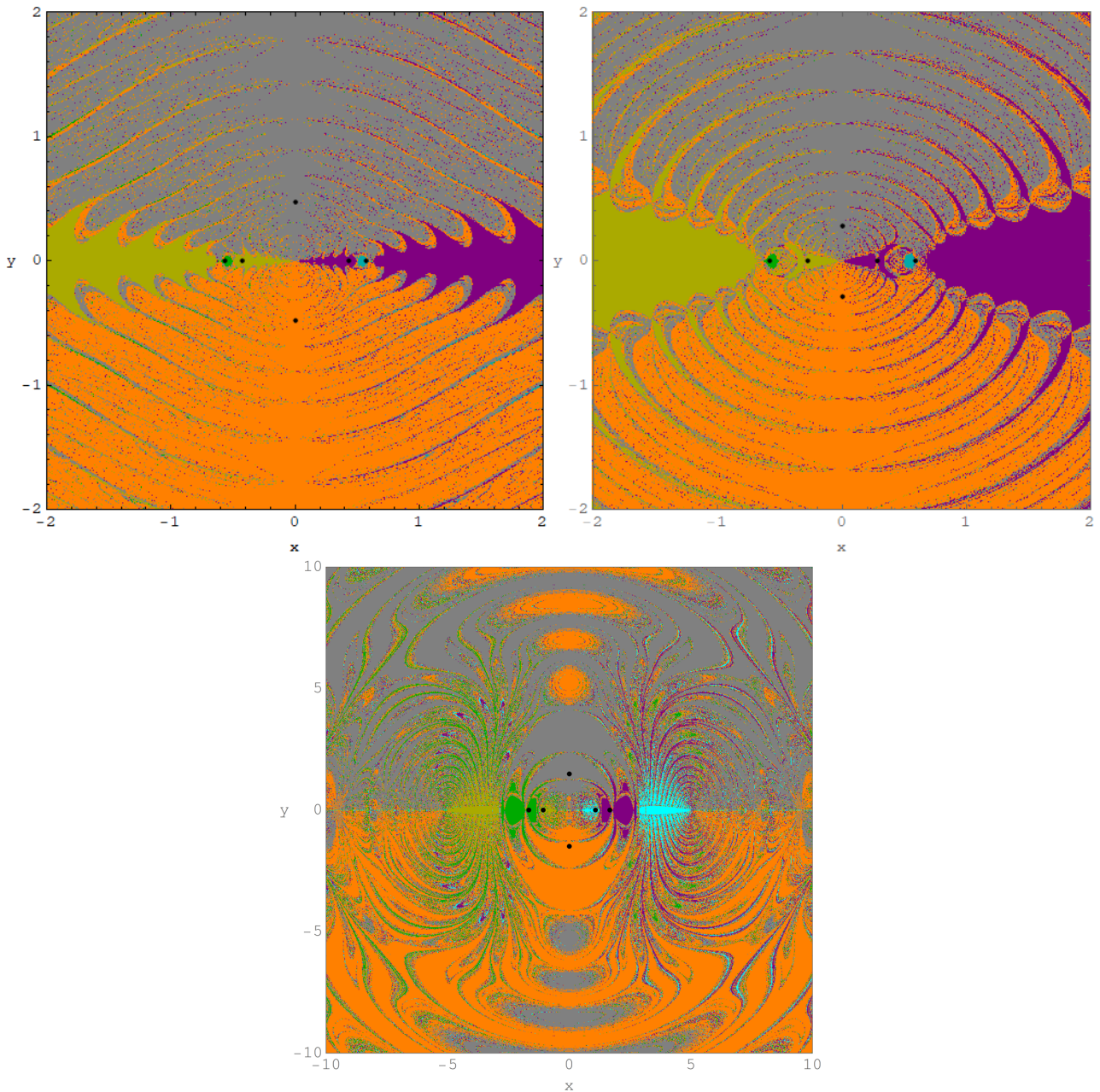


**Fig. 12** The BoC linked with the libration points on  $(x,y)$ -plane for  $\beta = 1000$ , and (a) for  $A = 0.025$ , (b)  $A = 0.75$ . For  $\beta = 0.1$ , and (c) for  $A = -0.215$ . The color codes for the BoC are as follows:  $L_{x1}^+ = \text{purple}$ ,  $L_{x2}^+ = \text{cyan}$ ,  $L_{x1}^- = \text{green}$ ,  $L_{x2}^- = \text{olive}$ ,  $L_{y1}^+ = \text{gray}$  and  $L_{y1}^- = \text{orange}$ . The dots show the positions of libration points. (colour figure online).

covered by BoC linked to the libration points  $L_{x4}^\pm$  and  $L_{y1}^\pm$ . However, the basin boundaries are composed of the mixture of the initial conditions and looks like chaotic sea. As the value of parameter  $A$  decreases from  $-0.005$  to  $-0.01$ , there is very few changes in the BoC linked to libration points. However, the legs and antennas of the exotic bugs decrease significantly which shows that the domain of the BoC decrease corresponding to libration points  $L_{x1}^-$  and  $L_{x1}^+$ . In Fig. 10c, the BoC is depicted for large scale of the configuration plane  $(x,y)$  to have the idea of the BoC on broader

scale. It can be noticed that multiple wings shaped region linked to the equilibrium points  $L_{x3}^\pm$  (magenta and brown) increases its wingspan and the boundaries of the basins looks highly chaotic, infact the area between the wings shaped region linked to  $L_{x3}^\pm$  and  $L_{y1}^\pm$  is highly chaotic which is composed of the mixture of various initial conditions. Therefore, it is very difficult to predict the final state of the initial conditions which falling in these chaotic reasons. As we compare the BoC with the previous panels we can notice that as the value of  $A$  decreases, the libration points  $L_{x3}^\pm$

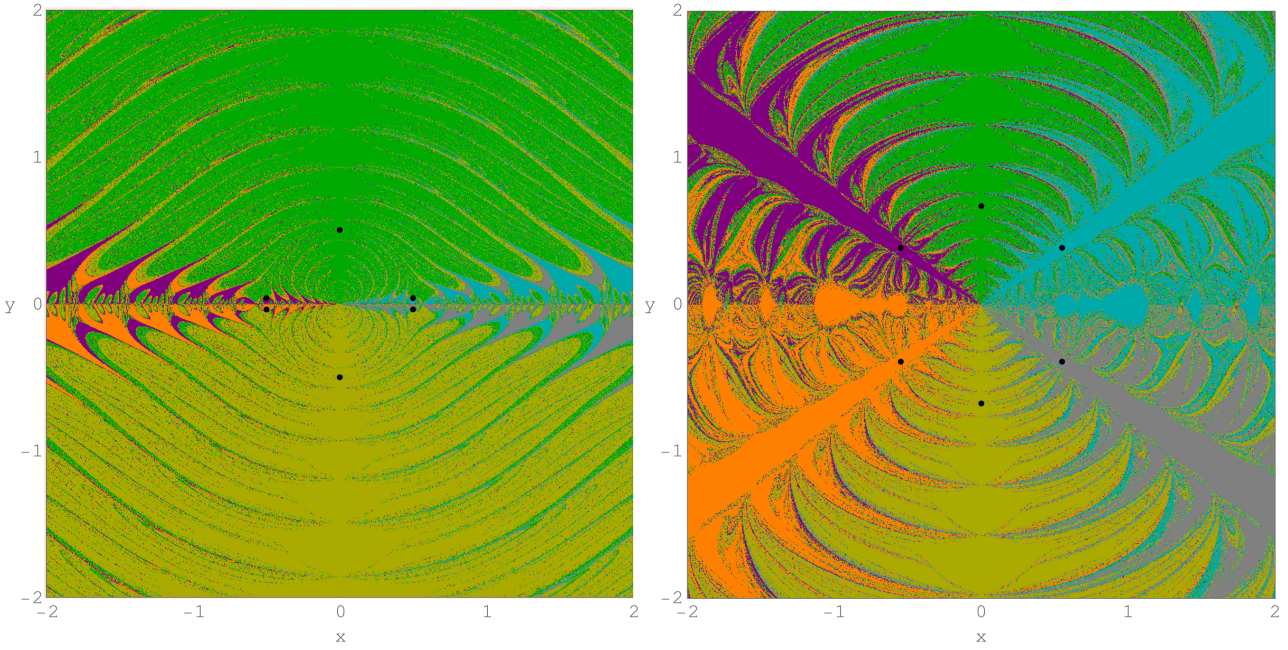


**Fig. 13** The BoC linked with the libration points on  $(x,y)$ -plane for  $\beta = 1000$ , and (a) for  $A = -0.097968$ , (b)  $A = -0.001$ . The color codes for the BoC are as follows:  $L_{xy1}^+ = \text{teal}$ ,  $L_{xy2}^+ = \text{purple}$ ,  $L_{xy1}^- = \text{gray}$ ,  $L_{xy2}^- = \text{orange}$ ,  $L_{y1}^+ = \text{green}$  and  $L_{y1}^- = \text{olive}$ . The dots show the positions of libration points. (colour figure online).

and  $L_{x4}^\pm$  come closer to each other respectively and consequently a major area of the domain of BoC of the configuration plane is covered by those initial conditions which converge to these libration points. The domain of the BoC corresponding to libration points  $L_{xyi}^\pm$ ,  $i = 1, 2$ , looks like four lobes originating from  $x$ -axis. The domain of the BoC linked to these libration points increase as the value of  $A$  decrease. In Fig. 10d, the BoC is illustrated for that value of  $A$  for which the libration points  $L_{x3}^\pm$  and  $L_{x4}^\pm$  collide and annihilate completely, and consequently only ten libration points exist. We noticed that a major area of the configuration plane looks like chaotic sea, composed of the initial conditions, however the areas in the neighbourhood of the equilibrium points are regular. If we compare panels Fig. 10a,b, to panel Fig. 10d, we notice that the area adjoining the exotic bugs shaped region which looks highly chaotic and appears elliptic in shape, increases significantly. We believe that the initial conditions which converge to libration points  $L_{x3,4}^\pm$  when these points exist, now converge randomly to any of the existing libration points which is the reason why this region turn into the chaotic sea. Infact, the regular island of BoC which converges to the equilibrium points  $L_{x3,4}^\pm$  turned into the chaotic sea. The zoomed view near the origin shows that a elongated "eight" shaped region exist from  $L_{x2}^-$  to  $L_{x2}^+$  is also chaotic except the four regular lobes shaped basins linked to  $L_{xyi}^\pm$ ,  $i = 1, 2$ .

In Fig. 11, the BoC is illustrated for fixed value of  $\beta = 1000$  and those values of  $A$  for which there exist ten equilibrium points. We noticed that in both the panels, the extent of

the BoC is infinite linked to all the equilibrium points. Moreover, as the value of  $A$  increases from  $-0.142$  to  $-0.09804989$ , the BoC linked to libration points  $L_{xyi}^\pm$ ,  $i = 1, 2$ , becomes more regular also the domain of the BoC linked to the equilibrium points  $L_{xi}^\pm$ ,  $i = 1, 2$ , decrease. However, in both the cases a major part of the configuration plane is covered by chaotic sea composed of the various initial conditions.

### 6.1.2 When libration points lie on axes only

In this subsection, we will discuss the BoC in those case for which the libration points lie only on the axes. In Fig. 12, we have discussed the BoC for two different values of  $\beta = 0.1, 1000$ , and different values of  $A$ . Fig. 12a, when  $\beta = 1000$  and  $A = 0.025$ , there exist four equilibrium points on  $x$ -axis while two equilibrium points on  $y$ -axis. We noticed that the configuration plane is covered by well-formed BoC which extended to infinity. However, the majority of the area is occupied by domain of the BoC linked to the equilibrium points  $L_{y1}^\pm$ , which looks like the multiple butterfly wings. In addition, the domain of BoC which exists in the vicinity of the equilibrium points  $L_{x1}^\pm$  looks like circular island and the domain of BoC linked with the collinear equilibrium points  $L_{x2}^\pm$  looks like lobes originate from origin along the  $x$ -axis. Further, as the value of the oblateness parameter  $A = 0.75$  (see Fig. 12b) increases, it is seen that the butterfly wings shaped regions shrink in the vicinity of  $x$ -axis and consequently domain of the BoC associated with the equilibrium points  $L_{x2}^\pm$  increases whereas there is negli-

gible change in the circular island shaped BoC linked with  $L_{x1}^{\pm}$ .

Fig. 12c, the BoC is illustrated for  $\beta = 0.1$  and  $A = -0.215$ . It is seen that the basin of convergence associated with the equilibrium points  $L_{x1}^{\pm}$  (see purple & green colors) looks like exotic bugs with many legs and antenna however, the BoC linked to libration points  $L_{x2}^{\pm}$  the two exotic bugs shaped region corresponding to each libration points (shown in cyan and olive color) exist in which one exists in the vicinity of the libration points and other exists adjacent to the domain of BoC linked to the equilibrium points  $L_{x1}^{\pm}$  and wings and antennas of these exotic bugs are very noisy. It is observed that these wings and antenna are chaotic mixture of the initial conditions which converge to different attractors and consequently it is almost impossible to predict that to which attractors these initial conditions are converging.

### 6.1.3 When collinear libration points do not exist

In this subsection, we have illustrated the BoC for fixed value of  $\beta$  and various values of  $A$  for which there exist only non-collinear libration points (see Fig. 13). The extent of the domain of BoC linked to each of the libration point is also infinite in these cases. When the value of  $A = 0.097968$ , majority of the areas of the configuration plane is covered by domain of BoC linked to the libration points  $L_{y1}^{\pm}$ . The well formed domain of the BoC linked to the libration points  $L_{xyi}^{\pm}$ ,  $i = 1, 2$ , exist in the vicinity of the  $x$ -axis. However, the entire configuration plane look like a chaotic sea of initial conditions except for those BoC which are associate to  $L_{xyi}^{\pm}$  (see Fig. 13a). The BoC changes drastically as the value of the  $A$  increase to  $A = -0.001$ . The regular domain of the BoC linked to the libration points  $L_{xyi}^{\pm}$  increases significantly and consequently the domain of the BoC linked to  $L_{y1}^{\pm}$  decreases. However, the basins boundaries are very noisy and, indeed, it is impossible to predict the final state of the initial condition falling inside these basins boundaries even after a sufficient number of iterations.

## 7 Concluding Remarks

In the present problem, the collinear restricted four body problem has been investigated where the peripheral primaries are non-spherical in shape. In particularly, the shape of the peripheral primaries are either oblate or prolate spheroid.

It should be emphasized that a numerical investigation is performed in such a thorough and systematic manner to unveil the effect of the parameters  $\beta$  and  $A$  on the position and stability of libration points, regions of possible motion and on the topology of BoC by applying the NR iterative scheme that all the illustrated results are novel, whereas they enhance substantially to our knowledge related to the evolution of the libration points.

The most important outcomes of our numerical analysis are listed below:

- The existence as well as the number of collinear libration points strongly depend on the particular values of parameters  $\beta$  and  $A$ . For  $\beta = 0.1$ , there exist eight collinear libration points for  $A \in (-0.039515, 0)$  while it reduces to four when  $A \in (-0.259259, -0.039515)$  and  $(0, 1)$ , in addition, for  $\beta = 1000$ , there exist four collinear equilibrium points when  $A \in (-0.166687, -0.09805989)$  and  $[0, 1)$  whereas there exist no collinear libration point for  $A \in (-0.09805989, 0)$ . It is further noticed that there exist two type of non-collinear libration points, i.e., the libration points which lie on  $(x, y)$  plane and the libration points which lie on  $y$ -axis for the considered values of  $\beta = 0.1, 1000$  and varying values of the parameter  $A$ .
- The movement of the libration points which lie on  $y$ -axis remains toward the central primary as the value of the parameter  $A$  increases. The libration points  $L_{xy1}^{\pm}$  and  $L_{xy2}^{\pm}$  originate in the vicinity of the libration point  $L_{x2}^{\pm}$  and move far from the  $x$ -axis along the arc shaped trajectories and again turned to annihilate in the neighbourhood of the peripheral primaries for  $A = 0$ .
- The stability analysis for the in-plane libration points suggests that only some of the libration points which lie on the  $x$ -axis are linearly stable for a particular value of  $\beta$  and particular range of the parameter  $A$ . Whereas none of the non-collinear libration points are found linearly stable for any permissible value of the parameter  $A$  for the studied value of  $\beta$ .
- The parametric evolution of the regions of possible motion in the in-plane case is illustrated and found that as the value of the Jacobian constant increases, the regions of the possible motion, where the test particle is free to move, decrease. Moreover, the region of forbidden motion decreases in the in-plane case when the value of  $A$  decreases.
- The evolution of the BoC as the function of the parameter  $A$  is presented to determine the effect of the parameter  $A$  on their topology. It is observed that in all the cases the extent of the domain of BoC linked to the libration points is infinite. The basins boundaries are always chaotic in nature which are mainly composed of those type of initial conditions which converge to any of the equilibrium points randomly.

We have used the latest version 12.0 of the Mathematica® to perform all numerical as well as graphical illustrations. We hope that the presented numerical analysis and the obtained results to be useful in the real world where the primaries are celestial bodies which are in collinear configuration. In future work it is interesting to unveil that how the topology of the BoC linked to the out-of-plane equilibrium points, if exists, is changed with the change when the value of parameters  $\beta$  and  $A$  changes.

## Compliance with Ethical Standards

- Funding: The author, Rajiv Aggarwal, has received the research grant by Department of Science and Technology, New Delhi, India.
- Conflict of interest: The authors declare that they have no conflict of interest.

## Acknowledgements

This work is funded by **Department of Science and Technology, India**, under project scheme **MATRICES (MTR/2018/000442)**.

## References

- Alvarez-Ramirez, M., E.Barrabés, M. Medina, M.Ollé: Ejection-Collision orbits in the symmetric collinear four-body problem, *Communications in Nonlinear Science and Numerical Simulation*, 71, 15(2019), 82-100. <https://www.sciencedirect.com/science/article/pii/S1007570418303484>
- Abouelmagd, E.I.: Existence and stability of triangular points in the restricted three-body problem with numerical applications. *Astrophysics and Space Science*, 342 (1), pp. 45-53, (2012). <https://link.springer.com/article/10.1007%2Fs10509-012-1162-y>
- Abouelmagd, E.I., Abdullah A. A., The motion properties of the infinitesimal body in the framework of bicircular Sun perturbed Earth-Moon system. *New Astronomy*, Volume 73, November 2019a, 101282. <https://doi.org/10.1016/j.newast.2019.101282>
- Abouelmagd, E.I., Garcia Guirao, J.L., Llibre, J.: Periodic orbits for the perturbed planar circular restricted 3-body problem. *Discrete and Continuous Dynamical Systems - Series B*, 24 (3), pp. 1007-1020, (2019b). <http://aimsciences.org/article/doi/10.3934/dcdsb.2019003>
- Arredondo, J.A., Guo, J., Stoica, C. et al.: On the restricted three body problem with oblate primaries. *Astrophys Space Sci* (2012) 341: 315. <https://doi.org/10.1007/s10509-012-1085-7>
- Arribas, M., Abad, A., Elipe, A., Palacios, M.: Equilibria of the symmetric collinear restricted four-body problem with radiation pressure. *Astrophys. Space Sci.* 361, 84 (2016). <https://link.springer.com/article/10.1007/s10509-016-2671-x>
- Arribas, M., Abad, A., Elipe, A., Palacios, M.: Out-of-plane equilibria in the symmetric collinear restricted four-body problem with radiation pressure. *Astrophys. Space Sci.* 361, 270 (2016). <https://link.springer.com/article/10.1007/s10509-016-2858-1>
- Asique, M. C. , Prasad, U. , Hassan, M. R., Suraj, M. S.: On the R4BP when third primary is an oblate spheroid. *Astrophys. Space Sci.* 357 (2015) 82. <https://doi.org/10.1007/s10509-015-2235-5>
- Asique, M. C. , Prasad, U. , Hassan, M. R., Suraj, M. S.: On the photogravitational R4BP when the third primary is a triaxial rigid body. *Astrophys. Space Sci.* 361 (2016) 379. <https://doi.org/10.1007/s10509-016-2959-x>
- Barrabés , E., Cors, J.M., Vidal, C.: Spatial collinear restricted four-body problem with repulsive Manev potential. *Celest. Mech. Dyn. Astron.* 129, 153-176 (2017). <https://link.springer.com/article/10.1007/s10569-017-9771-y>
- Baltagiannis, A.N., Papadakis, K. E.: Equilibrium points and their stability in the restricted four-body problem. *Int. J. Bifurc. Chaos* 21 (2011) 2179-2193. <https://doi.org/10.1142/S0218127411029707>
- Baltagiannis, A.N., Papadakis, K. E. : Families of periodic orbits in the restricted four-body problem. *Astrophys. Space Sci.* 336 (2011) 357-367. <https://doi.org/10.1007/s10509-011-0778-7>
- Douskos, C., Kalantonis, V., Markellos, P. et al.: On Sitnikov-like motions generating new kinds of 3D periodic orbits in the R3BP with prolate primaries. *Astrophys Space Sci* (2012) 337: 99. <https://doi.org/10.1007/s10509-011-0807-6>
- Douskos, C.N.: Collinear equilibrium points of Hills problem with radiation and oblateness and their fractal basins of attraction. *Astrophys. Space Sci.* **326**, 263–271 (2010)
- Hamilton, D. P.: Celestial mechanics: Fresh solutions to the four-body problem. *Nature*, 533 (2016) 187. <https://doi.org/10.1038/nature17896>
- Kalvouridis, T., Arribas, M., Elipe, A.: Dynamical properties of the restricted four-body problem with radiation pressure. *Mech. Res. Commun.* 33, 811-817(2006). <https://www.sciencedirect.com/science/article/pii/S0093641306000176>
- Kumari, B.S. , Kushvah, R.: Equilibrium points and zero velocity surfaces in the restricted four-body problem with solar wind drag. *Astrophys Space Sci* (2013) 344: 347. <https://doi.org/10.1007/s10509-012-1340-y>
- Leandro, E. S. : On the central configurations of the planar restricted four-body problem. *J. Differ. Equ.*, 226 (2006) 323-351. <https://doi.org/10.1016/j.jde.2005.10.015>
- Medvedev, Y.D., Perkov, N.I.: Restricted four-body problem. The case of a central configuration: libration points and their stability. *Astron. Lett.* 34 (2008) 357-365. <https://doi.org/10.1134/S1063773708050095>
- Michalodimitrakis, M.: The circular restricted four-body problem. *Astrophys. Space Sci.* 75 (1981) 289-305. <https://doi.org/10.1007/BF00648643>
- Maranhão, D. L., Llibre, J.: Ejection-collision orbits and invariant punctured tori in a restricted four-body problem. *Celest. Mech. Dyn. Astron.* 71 (1998) 1. <https://doi.org/10.1023/A:1008389427687>
- Palacios, M., Arribas, M., Abad, A. et al.: Symmetric periodic orbits in the Moulton-Copenhagen problem. *Celest Mech Dyn Astr* (2019) 131: 16. <https://doi.org/10.1007/s10569-019-9893-5>
- Selim, H.H., Guirao, J.L.G., Abouelmagd, E.I.: Libration points in the restricted three-body problem: Euler angles, existence and stability. *Discrete and Continuous Dynamical Systems -Series S*, 12 (45), pp. 703-710 (2019). <https://aimsciences.org/article/doi/10.3934/dcdss.2019044>
- Sharma, R.K. , Subba Rao, P.V.: Effect of oblateness on triangular solutions at critical mass. *Astrophys Space Sci* 60, 247 (1979). <https://doi.org/10.1007/BF00644329>
- Simmons, J.F.L., McDonald, A.J.C. , Brown, J.C.: The restricted 3-body problem with radiation pressure. *Celestial Mechanics* (1985) 35: 145. <https://doi.org/10.1007/BF01227667>
- Suraj, M.S., Zotos, E.E., Kaur, C., Aggarwal, R., et al., Fractal basins of convergence of libration points in the planar Copenhagen problem with a repulsive quasi-homogeneous Manev-type potential. *Int. J. Non-Linear Mech.*, **103**, 113-127, (2018b). <https://www.sciencedirect.com/science/article/abs/pii/S0020746218301240>
- Suraj, M.S., Mittal, A., Arora, M. et al., Exploring the fractal basins of convergence in the restricted four-body problem with oblateness. *Int. J. Non-Linear Mech.*, **102**, 62–71 (2018c). <https://www.sciencedirect.com/science/article/abs/pii/S0020746217308417>
- Suraj, M.S., Mittal, A., Aggarwal, R., Revealing the existence and stability of equilibrium points in the circular autonomous restricted four-body problem with variable mass, *New Astronomy*, **68** (2019) 1-9. <https://www.sciencedirect.com/science/article/pii/S1384107618302653>
- Suraj, M.S., Mittal, A., Kaur, C., Aggarwal, R., On the existence of libration points in the spatial collinear restricted four-body problem within frame of repulsive Manev potential and variable mass, *Chaos, Solitons and Fractals*, **117** (2018) 94-104. <https://www.sciencedirect.com/science/article/pii/S0960077918307082>



- Suraj, M.S., Aggarwal, R., Arora, M.: On the restricted four-body problem with the effect of small perturbations in the Coriolis and centrifugal forces. *Astrophys. Space Sci.* **362**, 159(2017a)
- Suraj, M.S., Asique, M.C., Prasad, U. et al.: Fractal basins of attraction in the restricted four-body problem when the primaries are triaxial rigid bodies. *Astrophys. Space Sci.* **362**, 211(2017b)
- Zotos, E.E., Suraj, M.S., Basins of attraction of equilibrium points in the planar circular restricted five-body problem, *Astrophys. Space Sci.*, **363** (2017) 20. <https://link.springer.com/article/10.1007/s10509-017-3240-7>
- Zotos, E. E.: Escape and collision dynamics in the planar equilateral restricted four-body problem. *Int. J. Nonlin. Mech.* 86 (2016) 66-82. <https://doi.org/10.1016/j.ijnonlinmec.2016.08.003>
- Zotos, E. E.: Revealing the basins of convergence in the planar equilateral restricted four-body problem. *Astrophys Space Sci.* (2017a) 362, 2. <https://doi.org/10.1007/s10509-016-2973-z>
- Zotos, E. E.: Equilibrium points and basins of convergence in the linear restricted four-body problem with angular velocity. *Chaos, Solitons and Fractals* (2017b) 101, 8-9. <https://www.sciencedirect.com/science/article/abs/pii/S0960077917301856>
- Zotos, E.E.: Classifying orbits in the restricted three-body problem. *Nonlinear Dyn* (2015a) 82: 1233. <https://doi.org/10.1007/s11071-015-2229-4>
- Zotos, E.E.: Crash test for the Copenhagen problem with oblateness. *Celest Mech Dyn Astr* (2015b) 122: 75. <https://doi.org/10.1007/s10569-015-9611-x>
- Zotos, E.E.: Comparing the escape dynamics in tidally limited star cluster models. *Monthly Notices of the Royal Astronomical Society*, (2015)452 (1): 193-209. <https://academic.oup.com/mnras/article/452/1/193/1750211>
- Zotos, E.E., Jung, C.: Orbital and escape dynamics in barred galaxies-III. The 3D system: correlations between the basins of escape and the NHIMs. *Monthly Notices of the Royal Astronomical Society*, (2018)473 (1):806-825. <https://academic.oup.com/mnras/article-abstract/473/1/806/4159380>
- Zotos, E.E., Dubeibe, F.L., González, G.A., : Orbit classification in an equal-mass non-spinning binary black hole pseudo-Newtonian system. *Monthly Notices of the Royal Astronomical Society*, (2018)477 (4): 5388-5405. <https://academic.oup.com/mnras/article-abstract/473/1/806/4159380>
- Zotos, E.E.: Fractal basins of attraction in the planar circular restricted three-body problem with oblateness and radiation pressure. *Astrophys. Space Sci.* **361**, 181 (2016)